

Powder processing, crystalline structure, sintering, and electrical properties of
 $\text{NdM}_{0.5}\text{Mn}_{0.5}\text{O}_3$ (M = Ni, Co, Cu) Manganites

C. Moure¹, J. Tartaj¹, V. Gil¹, O. Peña², P. Durán¹

¹Instituto de Cerámica y Vidrio (CSIC)-Campus de Cantoblanco, Camino de Valdelatas s/n, 28049 – Madrid, Spain.

²Chimie du Solide et Inorganique Moleculaire, UMR 6511. CNRS – Université de Rennes I, Institut de Chimie de Rennes, 35042 Rennes cedex, France.

ABSTRACT

Perovskite single-phase $\text{NdMe}_{0.5}\text{Mn}_{0.5}\text{O}_3$ (Me = Co, Ni, Cu) powders were achieved at low-temperature (600-700°C) by using the ethylene glycol-metal nitrate polymerized complex method. The structure of the perovskite system was investigated, and an orthorhombic structure O'-type was found for the Co-, Ni-, and Cu- containing perovskite materials. Replacement of Cu, Co, and Ni onto B-sites of the NdMnO_3 perovskite structure improve densification of pure manganite up to about 99 % of theoretical at temperatures as low as 960°C in the particular case of the $\text{NdCu}_{0.5}\text{Mn}_{0.5}\text{O}_3$ samples. The sintering enhancement of Cu-, Co- and Ni- containing perovskite materials is explained, assuming the no evidence for a low-temperature eutectic-liquid, as due to a change in the mechanism of the early stages of the densification process.

Electrical measurements have shown semiconducting behaviour for all the solid solutions. Thermally activated small polaron hopping mechanism controls the conductivity of these perovskite ceramics.

Keywords: Manganites, electrical properties, powder processing, sintering

1.-Introduction

Due to their phase stability and thermal expansion compatibility with YSZ in the cofiring process at high temperature, 1300 – 1400°C, lanthanum based perovskite systems, i.e., La_{1-x}

$x\text{A}_x\text{MnO}_3$ ($\text{A} = \text{Sr}$ and $x = 0.1$ to 0.4), have been used as cathode for high temperature SOFC system^{1,2}. However, such an asseveration has been strongly questioned by many authors which reported de reaction of the electrolyte YSZ with lanthanum of the perovskite³⁻⁷, with the formation of a pyrochlore phase $\text{La}_2\text{Zr}_2\text{O}_7$ which ionic conductivity ($10^{-4} \text{ S cm}^{-1}$) is three orders lower than that of YSZ ($10^{-1} \text{ S cm}^{-1}$) at the SOFC operating temperature ($\sim 1000^\circ\text{C}$). For those and many other reasons the last tendencies are addressed to the use of electrolytes, such as those based on doped – ceria, working at temperatures lower than $600 - 800^\circ\text{C}$, and having higher ionic conductivity than YSZ^{8,9}. However, such electrolyte has a thermal expansion coefficient much lower than the most of the Co – based perovskite cathodes. Therefore, the search of new compositions having the desirable properties for intermediate temperature SOFC applications is going on¹⁰.

Many attempts have carried out by substituting a divalent cation (Sr,Ca) for a trivalent cation (La) within A sites of the perovskite structure. Although such a substitution leads to the appearance of electronic holes in air, but a charge compensation of oxygen vacancies, at the same time that a high oxygen flux at moderate overpotentials was expected when using compositions such as $\text{La}_{1-x}\text{Sr}_x\text{Co}_{1-y}\text{Fe}_y\text{O}_3$ (LSCFe) as SOFC cathodes. These compositions have demonstrated higher electrical conductivity than LSM and to have high ionic conductivities and, therefore, they are assumed to be as promising SOFC cathode materials¹¹⁻¹³.

From the above, it could be concluded that rare earth manganite perovskite oxides have attracted much attention in recent years due to their incorporation as cathodes in high temperature SOFCs, and mainly the composition with La in the A-site have been extensively studied, while much less attention have been given to other rare earth manganites.

The purpose of the present work was to study other rare earth oxide systems as $\text{LnMe}_{1-x}\text{Mn}_x\text{O}_3$, where $\text{Ln} = \text{Nd}$ and ($\text{Me} = \text{Co}, \text{Ni}, \text{Cu}$) as possible cathode material for intermediate

temperature SOFCs. Replacement of lanthanum with neodymium on the A-site, and nickel, cobalt and copper on the B-site of the perovskite structure can provide a more stable system. In a first part, the powder preparation, crystallographic study, sintering behaviour, and electrical properties of the cathode materials prepared by the chemical polymerized complex method, is presented. The effect of Me-doping on these properties was examined.

2.-Experimental details

Ceramic powders of the composition $\text{NdMe}_{0.5}\text{Mn}_{0.5}\text{O}_3$ were prepared by the ethylene glycol-metal nitrate polymerized complex process¹⁴. The powder was calcined at 750°C for 2h, and then wet-milled with methanol in an attrition ball milling using zirconia balls. The crystallographic study was made at room temperature by X-ray diffraction (XRD) with a Siemens D5000 diffractometer ($\text{CuK}\alpha$ radiation) which operated at 40 kV and 30 mA. The XRD data were collected by step scanning in the range $20 < 2\theta < 75$. The lattice parameters were determined using a least squares unit cell refinement computer program.

After drying, the powders also were isostatically pressed (200 MPa). The compacts were then sintered in air by the constant rate of heating (CRH) with a dilatometer (model 402 E/7 Netzsch, Germany), and by the conventional ramp-and-holding methods. The heating and cooling rates were 2°C/min. The density of the sintered samples was measured by the Archimedes method in water. Microstructure of the samples was observed with a scanning electron microscope (SEM) on the gold-coated polished surfaces.

The electrical conductivity was measured on the sintered samples in air using an impedance-meter HP 4192 A by the standard two-point AC method upon cooling in the temperature range 25 to 400°C.

3.-Results and discussion

3.1. Powder characterization

After combustion the material has the black color which remained throughout all the powder processing. The simultaneous TG/DTA curves for the different prepared powder perovskites during heating of the dried polymeric gel between room temperature and 1000°C, revealed the same thermal features in all cases and, for clarity, only that corresponding to the NdCu_{0.5}Mn_{0.5}O₃ perovskite is shown in Fig. 1.

The TG curve showed a total weight loss of about 45 % up to 1000°C, which is due to the evolution of carbon compound as CO or CO₂, and nitrates in the form of N₂, NO, and NO₂. In the DTA curve the more relevant feature corresponded to that present at about 290°C, in which an abrupt exothermal peak, almost a line, which is due to the combustion reaction from the decomposition of the polymeric gel, was present.

The ethylene glycol-metal nitrate polymeric gel and calcined powders at different temperatures were also characterized by FTIR, not shown here. However, the appearance of IR absorption bands at about 2900, 1730, 1640 and 1400-1300, 1380,1330,1090-1040, and 500 cm⁻¹ are related to CH and CH₂ stretches, C=O stretching of residual acid groups, carbonaceous materials, NO₃⁻ ion stretching, OH or C-OH stretches, symmetric and antisymmetric stretches of C-O, and metal-oxygen bonds, respectively¹⁵. In the final reacted powders most of these IR bands disappeared, and only those assigned to the metal-oxygen bonds were still observed.

Figure 2 shows the XRD patterns of the dried polymeric gel, after the combustion reaction, and after calcining. The polymeric gel was amorphous and remained as such after the combustion reaction, i.e., the perovskite phase was not formed up to higher temperatures (> 600°C) indicating, thus, that the temperature reached during the ignition was not sufficient to crystallize the perovskite phase. After calcining at 750°C a well-crystallized perovskite phase was obtained and all the diffraction peaks could be indexed according to an orthorhombic Pbnm space group (GdFeO₃-type structure). The crystallographic data for the three

synthesized perovskite phases are given in Table 1. As it is well known, two types of orthorhombic structures are generally distinguished. The O-type structure, which is characterized by the relationship $a \leq c/(2)^{1/2} \leq b$, exists when the lattice deformation is relatively small, while the O'-type structure, with $c/(2)^{1/2} \leq a \leq b$, exists in the case of a relatively enhanced lattice deformation. According to these crystallographic data, it can be said that the lattice deformation by the replacement of Mn by the transition metal such as Co, Ni, and Cu on the B-site of the perovskite structure was relatively small. The existence of an O'-type structure in the three perovskite material, i.e., the same as in the pure NdMnO₃, supported such a statement. On the other hand, the orthorhombicity factor, b/a , is closer to unity in the sequence Co > Ni > Cu. We further assume a particle coordination number of 6 in all cases and, therefore, the cationic radii size¹⁶ sequence Co²⁺ (0.745 Å) > Cu²⁺ (0.73 Å) > Ni²⁺ (0.69 Å) > Mn³⁺ (0.645 Å) is in some contradiction with the above b/a variation.

The specific surface areas measured by the nitrogen adsorption, using a three point BET analysis, were 13.5, 20, and 10 m²g⁻¹ after calcining at 750°C for 2h. The particle (agglomerate) size calculated from the BET analysis using the equation $d_{\text{BET}} = 6/S\rho$, where ρ is the crystallographic density of the powder were about 62, 41, and 82 nm for the perovskite powders NdCo_{0.5}Mn_{0.5}O₃, NdNi_{0.5}Mn_{0.5}O₃, and NdCu_{0.5}Mn_{0.5}O₃, respectively. These results indicated, a) that this synthesis method successfully leads to perovskite single-phase powders, and b) the obtained powders are in the nanosize range and, therefore, they are highly sinterable.

3.2.Sintering and microstructural development

Green compacts were prepared from powders calcined at 750°C and sintered up to 1450°C in air, by the CRH method. Figure 3 shows the linear shrinkage rate ($d(dL/L_0) / dT$) as a function of temperature for the different perovskite materials.

It can be observed from this figure that the substitution of Mn by Cu in the perovskite structure shifts the onset of sintering towards lower temperatures than with Co or Ni and, moreover, the addition of Cu decreases the temperature of maximum shrinkage rate (T_m) significantly. For example, T_m decreases from 1300°C for pure NdMnO₃ perovskite to 960°C for NdCu_{0.5}Mn_{0.5}O₃, i.e., almost 350°C lower. In the case of the Co substitution such a decreasing in T_m was of only 100°C, and in the case of Ni substitution T_m was slightly higher than that for the pure perovskite material. Furthermore, it must be noted that the width of the shrinkage temperature range also decreases, and for Cu-, Co-, and Ni-containing perovskite materials is much narrower. Such a behaviour could be considered as a typical phenomenon present in a liquid phase-assisted densification process¹⁷, at least, in the case of the Cu and Co replacement. However, the no evidence for a low-temperature eutectic point in the Nd-Me-Mn ternary oxides system, is suggesting that the fast densification rate in Cu-, and Co-perovskite materials could not be related to liquid-phase sintering and, therefore, another different mechanism predominates, at least in the early stages of sintering.

The microstructure of the NdNi_{0.5}Mn_{0.5}O₃ sample sintered at 1450°C (90% dense), as shown in the figure 4a was very uniform, with a small grain size, (~1µm). Figure 4b shows the microstructure of the NdCo_{0.5}Mn_{0.5}O₃ sample after sintering at 1350°C, (94% dense). Many trapped pores within the grains were present as consequence of the oxygen loss during the reduction process of Co₃O₄ to CoO at high temperatures. At higher magnification, no shown here, a twinning domain phenomenon on the grain surfaces was present, which is typical of a structure transition occurring on cooling. The grain size was ~5µm, with a quite uniform grain size distribution. NdCu_{0.5}Mn_{0.5}O₃ sample sintered at 1000°C, (98% dense) did not shows any twinning phenomenon and the grain size was quite small, (~1.5µm), as it is shown in the figure 4c. From these microstructural features it can be said that the Ni²⁺ cations inhibited the grain growth process.

3.3. Electrical conductivity

Table 2 resumes the values of some electrical parameters corresponding to the three compositions. The activation energy of samples containing Co and Ni is higher than that of the Cu sample. This fact explains the lower values of conductivity of those compositions at room temperature and the higher ones at 400°C. All the samples showed an small polaron hopping thermally activated as conductivity mechanism, according to the ρT vs $1/T$ curves, not represented here.

4.-Conclusions

Perovskite single-phase $\text{NdMe}_{0.5}\text{Mn}_{0.5}\text{O}_3$ (Me = Co,Ni,Cu) powders were achieved at low-temperature (600-700°C) by using the ethylene glycol-metal nitrate polymerized complex method. The structure of the perovskite system was investigated, and an orthorhombic structure O'-type was found for the Co-, Ni-, and Cu- containing perovskite materials. Replacement of Cu, Co, and Ni onto B-sites of the NdMnO_3 perovskite structure improve densification of pure manganite up to about 99 % of theoretical at temperatures as low as 960°C in the particular case of the $\text{NdCu}_{0.5}\text{Mn}_{0.5}\text{O}_3$ samples. The sintering enhancement of Cu-, Co- and Ni- containing perovskite materials is explained, assuming the no evidence for a low-temperature eutectic-liquid, as due to a change in the mechanism of the early stages of the densification process. Electrical measurements have shown semiconducting behaviour for all the solid solutions. Thermally activated small polaron hopping mechanism controls the conductivity of these perovskite ceramics.

Acknowledgements

The present work was supported by Project 07N/0096/02 of the Autonomous Community of Madrid °(CAM).

5.-References

1. Minh, N.Q., Ceramic fuel cells., J.Am.Ceram.Soc., 1993, 76, 563.
2. Yamamoto, Y., Takeda, Y., Kanno, R., Kojima, T., Perovskite-type oxides as oxygen electrodes for high temperature solid oxide fuel cells, Solid State Ionics., 1987, 22, 241.
3. Lau, S.K. Singhal, S.C., Potential electrode/electrolyte interactions in solid oxide fuel cells, Corrosion 85, Paper Number 345, Boston MS, 1985.
4. Taimatu, H. Wada, K. Kaneko, H., Mechanism of reaction between lanthanum manganite and YSZ, J.Am.Ceram.Soc., 1992, 75, 401.
5. Yokokawa, H. Saka, N. Kawada, T. Dokiya, M., Thermodynamic analysis on interface between perovskite electrode and YSZ electrolyte, Solid State Ionics, 1990, 40/41, 398.
6. Yamamoto, O. Takeda, Y. Kanno, R. Kojima, T. Stability of perovskite oxide electrode with stabilized zirconia, Proceedings of the First Internal Symp. on SOFCs, in: S.C. Singhal (Edit), The Electrochemical Society, Pennington, NJ, 1989, p. 242.
7. Takeda, Y. Nakai, S. Kojima, T. Kanno, R. Imanishi, N. Shen, G.D. Yamoto, O. Mori, M. Abe, T. Electrical and mechanical properties of zirconia-alumina composite electrolyte, Mat. Res.Bull., 1991, 26, 153.
8. Mogensen, M. Lindegaard, T. Hansen, U.R., Physical properties of mixed conductor solid oxide fuel cell anodes of doped CeO₂, J.Electrochem.Soc., 1994, 41, 2122.
9. Navarro, L.M. Marques, F.M.B. Frade, J.R., n-Type conductivity in Gadolinia-doped ceria, J.Electrochem.Soc., 1997, 144, 267.
10. Carter, S. Selcuk, S. Chater, R.J. Kajda, J. Kilner, J.A., Oxygen transport in selected nonstoichiometric perovskite-structure oxides, Solid State Ionics., 1992, 53/56, 597.
11. Tai, L.W. Nasrallah, M.M. Anderson, H.U. Sparlin, D.M. Schlin, S.R., Structure and electrical properties of La_{1-x}Sr_xCo_{1-y}Fe_yO₃. Part I The system La_{0.8}Sr_{0.2}Co_{1-y}Fe_yO₃, Solid State Ionics, 1995, 76, 259.

12. Tai, L.W. Nasrallah, M.M. Anderson, H.U. Sparlin, D.M. Schlin, S.R. , Structure and electrical properties of $\text{La}_{1-x}\text{Sr}_x\text{Co}_{1-y}\text{Fe}_y\text{O}_3$. Part II, *Solid State Ionics*, 1995, 76, 273.
13. Maguirre, E. Gharbage, B. Marques, F.M.B. Labrincha, J.A., Cathode materials for intermediate temperature SOFCs, *Solid State Ionics*, 2000, 127, 329.
14. Duran, P. Tartaj, J. Rubio, F. Peña, O. Moure, C., Preparation and powder characterization of spinel-type $\text{Co}_x\text{NiMn}_{2-x}\text{O}_4$ ($0.2 < x < 1.8$) by the ethylene glycol-metal nitrate polymerized complex process, *J.Europ.Ceram.Soc.*, 2004, 24, 3035.
15. Nakamoto, K. *Infrared and Raman Spectra of Inorganic and Coordination compounds*, 4th ed. Wiley Press, New York, 1986.
16. Shanon, R.D., Prewitt C.T., Effective ionic radii in oxides and fluorides, *Acta Crystallogr. A* 32, 1976, 751.
17. Kingery, W.D., Bowen, H.K., Uhlmann, D.R. *Introduction to Ceramics*, 2nd edition, Wiley, NY, 1976.

Table 1. Phase symmetry, lattice parameters, unit cell volume, orthorhombicity, and type of orthorhombic structure of the NdMe_{0.5}Mn_{0.5}O₃ manganites. Pure Nd manganite is included for comparison

Samples	Symmetry	a(nm)	b(nm)	c(nm)	Vol (nm ³)	b/a	T.of orth.struct
NdMnO ₃	Orthorhom	0.5408	0.5788	0.7555	0.2364	1.07	O'-type
NdNi _{0.5} Mn _{0.5} O ₃	Orthorhom	0.5428	0.5560	0.7510	0.2267	1.024	O'-type
NdCo _{0.5} Mn _{0.5} O ₃	Orthorhom	0.5433	0.5579	0.7527	0.2281	1.027	O'-type
NdCu _{0.5} Mn _{0.5} O ₃	Orthorhom	0.5429	0.5564	0.7599	0.2297	1.025	O'-type

Table 2.
Electrical parameters of sintered samples

Samples	σ_{27} (S*M ⁻¹)	σ_{400} (S*M ⁻¹)	E _a (eV)
NdNi _{0.5} Mn _{0.5} O ₃	8.43	88.42	0.11
NdCo _{0.5} Mn _{0.5} O ₃	10.33	89.53	0.10
NdCu _{0.5} Mn _{0.5} O ₃	13.83	62.25	0.073

FIGURE CAPTIONS

Figure 1. TG and DTA curves corresponding to the gel precursor of the $\text{NdCu}_{0.5}\text{Mn}_{0.5}\text{O}_3$ composition

Figure 2. Evolution of X-Ray patterns of a polymerised gel as a temperature function

Figure 3. Linear shrinkage rate as a function of temperature for the different perovskite materials

Figure 4. Micrographies of sintered samples, a) Ni sample, b) Co sample, c) Cu sample

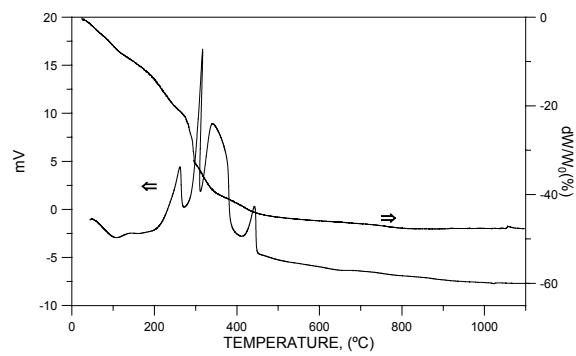


Figure 1.

C. Moure¹, J. Tartaj¹, V. Gil¹, O. Peña², P. Durán¹

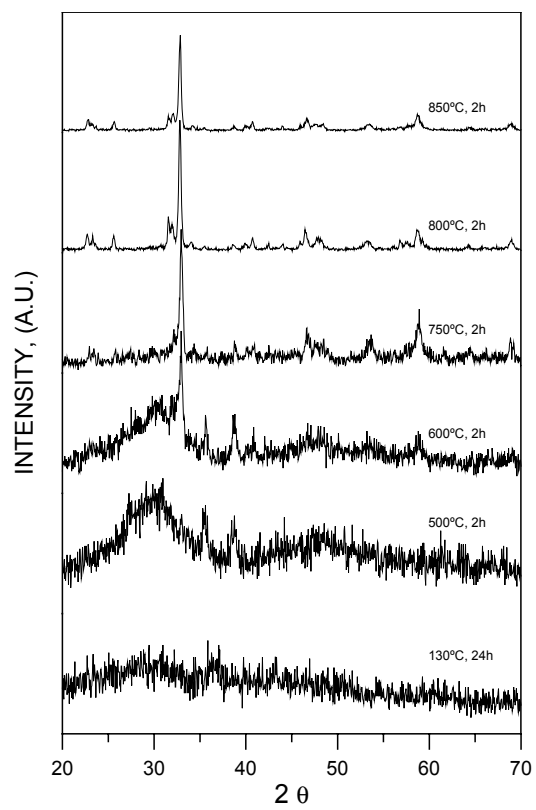


Figure 2

C. Moure¹, J. Tartaj¹, V. Gil¹, O. Peña², P. Durán¹

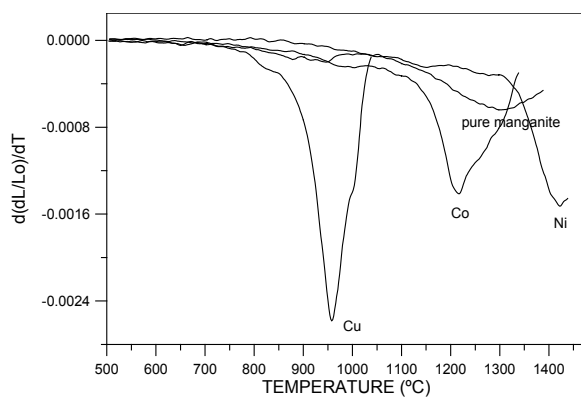
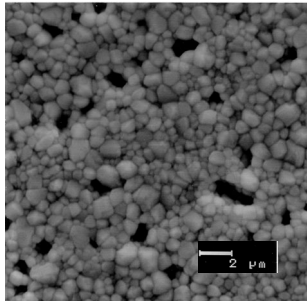
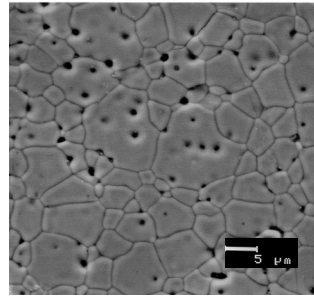


Figure 3

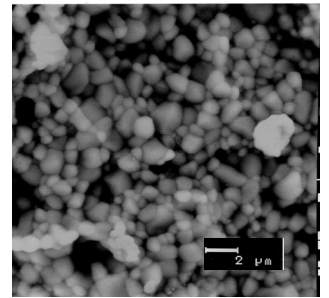
C. Moure¹, J. Tartaj¹, V. Gil¹, O. Peña², P. Durán¹



a



b



c

Figure 4

C. Moure¹, J. Tartaj¹, V. Gil¹, O. Peña², P. Durán¹